SERI/TP-217-3413
UC Category: 261
DE89000835

Prediction of Stochastic Blade Responses Using a Filtered Noise Turbulence Model in the FLAP Code

R. W. Thresher
W. E. Holley
A. D. Wright

November 1988

Prepared for the Eighth ASME
Wind Energy Symposium
Houston, Texas
22-25 January 1989

Prepared under Task No. WE811202

Solar Energy Research Institute
A Division of Midwest Research Institute

1617 Cole Boulevard
Golden, Colorado 80401-3393

Prepared for the
U.S. Department of Energy
Contract No. DE-AC02-83CH10093

NOTICE

This report was prepared as an account of work sponsored by an agency of the United States government. Neither the United States government nor any agency thereof, nor any of their employees, makes any warranty, express or implied, or assumes any legal liability or responsibility for the accuracy, completeness, or usefulness of any information, apparatus, product, or process disclosed, or represents that its use would not infringe privately owned rights. Reference herein to any specific commercial product, process, or service by trade name, trademark, manufacturer, or otherwise does not necessarily constitute or imply its endorsement, recommendation, or favoring by the United States government or any agency thereof. The views and opinions of authors expressed herein do not necessarily state or reflect those of the United States government or any agency thereof.

Printed in the United States of America
Available from:
National Technical Information Service
U.S. Department of Commerce
5285 Port Royal Road
Springfield, VA 22161

Price: Microfiche A01
Printed Copy A02

Codes are used for pricing all publications. The code is determined by the number of pages in the publication. Information pertaining to the pricing codes can be found in the current issue of the following publications which are generally available in most libraries: *Energy Research Abstracts (ERA)*; *Government Reports Announcements* and Index (*GRA* and I); *Scientific and Technical Abstract Reports (STAR)*; and publication NTIS-PR-360 available from NTIS at the above address.

PREDICTION OF STOCHASTIC BLADE RESPONSES USING A FILTERED NOISE TURBULENCE MODEL IN THE FLAP CODE

R. W. Thresher
Solar Energy Research Institute
Golden, Colorado

W. E. Holley
U.S. Windpower, Inc.
Burlington, Massachusetts

A. D. Wright
Solar Energy Research Institute
Golden, Colorado

ABSTRACT

The wind turbine structural dynamics model, FLAP (Force and Loads Analysis Program), has been modified to include turbulent wind fluctuations based on a filtered-noise model. The importance of including the effects of turbulent wind fluctuations in the structural-loads predictive model has long been recognized. These stochastic loads are the dominant fatigue loads for many structural components in horizontal-axis wind turbines.

The turbulence field at the rotor plane is approximated by interpolating functions, which allow the velocity field to vary quadratically for velocity components normal to the rotor plane and linearly for in-plane velocity components. The velocity field represented in this fashion is constructed to vary randomly with time and space and give the proper correlation between spatial locations and velocity components. For the normal velocity components, the spectral representations of these velocity fluctuations approximate those observed from a rotating turbine blade up to a frequency of two times per rotor revolution (2P). For the less-important in-plane components, the spectral representations approximate those observed from a rotating turbine blade up to 1P.

The time-domain model described in this paper uses a random number generator to construct a white-noise time series with uniform spectral density over the frequency range of interest. This signal is then filtered to obtain the various wind fluctuations, which are used as input to the FLAP code. This requires as input only the mean wind speed, the turbulence intensity, and an estimate for the integral scale. The modeling is based on the assumptions that the velocity fluctuations are statistically stationary, homogeneous, and isotropic, and satisfy Taylor's frozen field hypothesis. The von Karman model is used to characterize the correlation between velocities of points separated in space.

To gain insight into the usefulness of this turbulence simulation for predicting stochastic turbine loads, the FLAP code was used to model three data cases from the 1986 testing done on the Howden 330-kW turbine. The FLAP code was run with the wind turbulence parameters set to model the actual test conditions to generate simulated time series of bending moments. The response spectra calculated from these time series were then compared with the experimental measurements obtained from the field test. Comparing the simulation results with actual test measurements generally shows good agreement.

It takes about an hour to run a 450-revolution FLAP simulation using an 80386-based personal computer (PC) running at 20 MHz. The required knowledge of the actual turbulence characteristics is modest. The mean wind speed and the turbulence intensity are easily computed from time-series wind data. As discussed here, the integral scale of the turbulence can be estimated from calculations of the longitudinal wind spectrum. This type of simulation should become part of the process of designing wind turbines. It produces time-series results that can be used to determine peak loads, and it can be rainflow-counted for estimating fatigue damage rates. In addition, the computational and data input requirements are within the means of even the smallest design team.

INTRODUCTION

Accurately predicting wind turbine blade loads and resulting stresses is important for predicting the fatigue life of components. There is a clear need within the wind industry for validated codes that can predict not only the deterministic loads from the mean wind velocity, wind shear, and gravity, but also the stochastic loads from turbulent inflow. The FLAP code has already been validated for predicting deterministic loads (1,2). This paper concentrates on validating the FLAP code for predicting stochastic turbulence loads using the filtered-noise turbulence model, developed in (3), as input.

THE FILTERED-NOISE TURBULENCE MODEL

Because the blades of a horizontal-axis wind turbine rotate through the wind velocity field, fluctuations in the velocity seen from a moving blade occur at frequencies that are multiples of the rotation rate (1P, 2P, etc.). This effect can be understood by considering a wind velocity field that varies over the rotor disk but does not vary with time. As a wind turbine blade moves through this field, it encounters different velocities. After one complete revolution, the cycle is repeated, leading to a periodic velocity fluctuation. In the actual case, the time varying velocity field is convected past the wind turbine by the mean flow so that the fluctuations are no longer exactly periodic. However, the rotation frequency of the rotor is usually much greater than those typical frequencies in the fluctuating wind velocity observed at a stationary point; consequently, the eddy structure in the turbulence will remain highly coherent for several rotor revolutions as it passes the wind turbine. Therefore, the wind velocity seen by the rotating blade will have strong fluctuations at a band of frequencies near the integer multiples of the rotation rate. The spectral density will locally appear as a wide band process with an amplitude sinusoidally modulated at multiples of the rotation frequency. This rotational effect was described in (4) and was modeled by Kristensen and Frandsen (5), whose work was based on the earlier work of Rosenbrock (6).

There are essentially two approaches to modeling the three-dimensional correlation structure of atmospheric turbulence. In the first, or "hydrodynamic" approach, the fluctuating flow field is assumed to be homogeneous, isotropic, and incompressable. The theory of such a field is described in (7); the correlation structure or its Fourier transform, the spectral density, is completely described by a single function, usually given in the frequency domain by the energy spectrum. von Karman (8) suggested a particular form for the energy spectrum that fits the inertial subrange described in (9) and approaches a constant spectral density at low frequencies. This theory is widely used in aircraft flight control and structural-dynamics applications (10).

In the second, more empirical approach, the spectral densities of the velocity components are given by an empirical form [such as in (11)], and the coherencies between velocities at different points are given by the Davenport model (12). This approach is often used in dynamic analyses involving wind excitations of large structures such as towers, smoke stacks, and bridges (13). It has also been used for wind turbine structures by Sundar and Sullivan (14) and by Veers (15). Dragt (16) also used the Davenport coherency model but introduced an expansion of the periodic, rotating coherency function in Fourier series. Madsen (17) also used the Fourier series approach but modified the form of the Davenport coherency function to eliminate the dips in the rotating spectra at multiples of the rotor passage frequency described by Dragt. These dips have not been observed experimentally, and they result from the inadequacy of the Davenport model for frequencies below the limit of the inertial subrange [as pointed out by Kristensen and Jensen (18)]. These approaches have provided useful results but lead to certain difficulties. First, the impirical parameters for the coherency function must be determined for each site, requiring multiple correlations among spatially separated anemometers. Second, only the longitudinal velocity component (normal to the rotor disk) is modeled. Third, the incompressible flow condition is not satisfied. For these reasons, the hydrodynamic approach using the von Karman isotropic model was adopted as the basis for the turbulence model reported here.

Series Approximation for the Rotor Disk Turbulence Field

Consider a disk in the vicinity of the rotor of a horizontal-axis wind turbine. The coordinate system used is shown in Figure 1. The undisturbed wind velocity is assumed to vary a small amount over the region

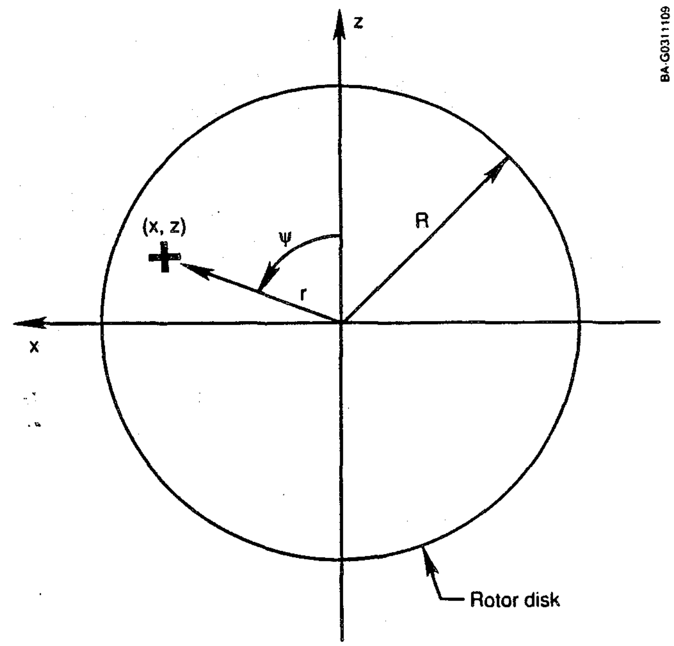

Fig. 1. Rotor disk coordinate system

of the rotor disk. Thus, an approximation in terms of simple analytical functions is appropriate. Consider first the velocity component normal to the plane of the rotor disk. Retaining all terms, including quadratic variations across the rotor disk of radius R, gives

$$\begin{aligned} v_y = V_y(t) &+ V_{y,x}(t)\, r\sin\psi + V_{y,z}(t)\, r\cos\psi \\ &+ V_{y,rr}(t)(r^2 - 1/2\, R^2) + V_{y,rs}(t)\, r^2 \sin 2\psi \\ &+ V_{y,rc}(t)\, r^2\cos 2\psi \end{aligned} \tag{1}$$

The functions $f_1 = 1,\ f_2 = r\sin\psi,\ f_3 = r\cos\psi,$ (2)

$$f_4 = r^2 - 1/2\, R^2,\ f_5 = r^2\sin 2\psi, \text{ and}$$

$$f_6 = r^2\cos 2\psi$$

are chosen to retain all quadratic variations and give the property of mutual orthogonality over the domain of the rotor disk. Thus,

$$\int_{\text{Disk}} f_j\, f_k\, dA = 0 \qquad \text{for } j \neq k\ .$$

In this case, it is possible to determine the terms v_y, which minimize the total square error over the rotor disk in terms of the true velocity. Using the usual generalized Fourier expansion, formulas of the following form are found:

$$V_y = \frac{1}{\pi R^2} \int_{\text{Disk}} v_y\, dA\ ;\ V_{y,x} = \frac{4}{\pi R^4} \int_{\text{Disk}} v_y\, r\sin\psi\, dA\ ;\ \text{etc.} \tag{3}$$

The complete results are given in (19).

Similar terms can also be derived for the in-plane velocity components. However, in this case we retain only linear variations across the rotor disk. Because the in-plane components are only of secondary importance in calculating wind turbine blade loads, the considerable simplification afforded by neglecting the quadratic and higher-order terms seems to be justified. Although the in-plane velocity components have only a small influence on blade loads, they may contribute significantly to the rotor yaw loads in some situations. The two in-plane velocity components are thus approximated by

$$v_x \approx V_x(t) + [\bar{\varepsilon}(t)-\varepsilon(t)]\, r\sin\psi + [\bar{\gamma}(t) - \gamma(t)]\, r\cos\psi$$

$$v_z \approx V_z(t) + [\bar{\gamma}(t) + \gamma(t)]\, r\sin\psi + [\bar{\varepsilon}(t)+\varepsilon(t)]\, r\cos\psi \qquad (4)$$

The six terms appearing in Eq. (4) are given by equations similar to Eq. (3) and can be found in (20).

Once all twelve terms are specified, it is possible to compute the correlation relations among them using the von Karman correlation model. As an example, consider the autocorrelation function for the term $V_y(t)$. Direct application of the first of Eqs. (3) gives

$$E[V_y(t+\tau)V_y(t)] = \frac{\sigma^2}{\pi^2 R^4} \int_{D2}\int_{D1} \left[f(\xi) + \frac{1}{2}\xi f'(\xi)\frac{\eta^2}{\xi^2}\right] dA_1 dA_2 \qquad (5)$$

where

$\xi^2 = \eta^2 + V^2\tau^2$

$\eta^2 = r^2 + \rho^2 - 2r\rho\cos(\Psi-\phi)$

$dA_1 = r\,dr\,d\psi$

$dA_2 = \rho\, d\rho\, d\phi$

r,ψ = polar coordinates in D1 (Disk 1)

ρ,ϕ = polar coordinates in D2 (Disk 2)

$f(\xi)$ = von Karman correlation function:

$$\sigma^2\beta\left(\frac{\xi}{\alpha L}\right)^{1/3} K_{1/3}\left(\frac{\xi}{\alpha L}\right)$$

$f'(\xi) = \frac{d}{d\xi} f(\xi)$

$\alpha = \dfrac{\Gamma(1/3)}{\sqrt{\pi}\,\Gamma(5/6)}$ (≈ 1.339)

$\beta = \dfrac{2^{2/3}}{\Gamma(1/3)}$ (≈ 0.5925)

σ = standard deviation of the velocity components

L = integral scale parameter $= \int_0^\infty f(\xi)d\xi$

$K_{1/3}(\cdot)$ = modified Bessel function of order 1/3

$\Gamma(\cdot)$ = gamma function.

The terms D1 and D2 refer to the positions of the rotor disk relative to the air mass at times t and $t + \tau$, respectively. Unfortunately, the integrations needed in Eq. (5) cannot be carried out analytically. However, if the velocities are scaled by the standard deviation σ, time is scaled by the ratio L/V, and length is scaled by the radius R of the rotor disk, the resulting correlation function becomes a nondimensional family depending on the single parameter R/L.

To more fully understand how to use these results, consider the case of filtered white noise. A stochastic differential equation describing filtered noise is given by

$$\dot{x} + ax = bw \qquad (6)$$

where w = the white-noise excitation
x = the filtered response
a,b = model parameters.

The autocorrelation function for the filtered response is exponential [as in (21)] and is given by

$$R_x(\tau) = E[x(t+\tau)x(t)] = \frac{b^2 S_w}{2a} e^{-a|\tau|} \qquad (7)$$

where S_w is the constant power spectral density of the white-noise excitation. In addition, using the definition of the spectral density function gives

$$S_x(\omega) = \frac{1}{2\pi} \int_{-\infty}^{\infty} [x(t)x(t+\tau)]\, e^{-i\omega\tau} d\tau \qquad (8)$$

and for the white-noise process of Eq. (6) this gives

$$S_x(\omega) = \frac{1}{2\pi}\frac{b^2 S_w}{(a^2 + \omega^2)} \qquad (9)$$

where ω is the radian frequency and, for convenience, $S_w = \frac{\sigma^2 L}{V^3}$.

To develop a simple set of simulation equations, each of the time-dependent coefficients in the inflow turbulence field Eqs. (1) and (4) are approximated by the stochastic differential equation described by Eq. (6). The parameters a and b for each of these equations are selected such that the autocorrelation functions approximate that required by the von Karman isotropic correlation model of Eq. (5). Thus, for the uniform velocity fluctuation term $V_y(t)$ of Eq. (1), it is required that

$$R_{V_y}(\tau) = E[V_y(t+\tau)V_y(t)] \approx \frac{b^2 S_w}{2a} e^{-a|\tau|} \qquad (10)$$

The left-hand side of this equation is determined from a numerical evaluation of Eq. (5). As previously noted, by properly scaling the velocities, time, and length, the autocorrelation function $R_{V_y}(\tau)$ can be written as a nondimensional family depending only on R/L. Thus, a and b can be reduced to a similar dependence. This same approach is used to determine the a and b values for each of the time-dependent coefficients in Eqs. (2) and (4). The resulting 24 a and b filter coefficients are given in Table 1 as a function of L/R and the scaling variables.

So far, we have discussed only the autocorrelation characteristics of the various terms in the velocity field approximation. What about the cross-correlation characteristics? Fortunately, because of the assumed isotropy of the model and the orthogonal properties of the functions $f_1 \ldots f_6$ in Eq. (9), most of the 12 terms in the velocity approximation are entirely uncorrelated. It turns out that there is a small correlation between V_y and $V_{y,rr}$ and a more important relation between V_y and the in-plane dilation term $\bar{\varepsilon}$. This latter relation arises as a consequence of mass continuity. The $\bar{\varepsilon}$ term is a radial flow term in the plane of the rotor for horizontal-axis wind turbines and contributes almost nothing to the aerodynamic forces. These two correlations are neglected for this model.

The development and discussion of the turbulent inflow modeling presented here have been by necessity brief. The reader interested in a more detailed development is referred to (3) and (20).

Table 1. Filter Coefficients

No.	Term	Coefficient Equation*
1	V_y	$a_1 = (1 - 1.713\ (R/L)(1. - .0790\ R/L)/(1 + 2.048\ R/L))(V/L)$ $b_2 = (1.414 - 2.713\ (R/L)(1 + .0159\ R/L)/(1 + 2.051\ R/L))(V^2/L)$
2	$V_{y,rr}$	$a_2 = (1.091\ L/R + .0276 + .0686\ R/L)(V/L)$ $b_2 = (.5508\ (R/L)^{-.25} + .6473 - .1365\ R/L)(V^2/LR^2)$
3	$\bar{\varepsilon}$	$a_3 = (1.654\ L/R + 1.069 + 2.154\ R/L)(V/L)$ $b_3 = (.3546\ (R/L)^{-.25} + .3951 + .2593\ R/L)(V^2/LR)$
4	$V_{y,z}$	$a_4 = (.3266\ L/R + .5953 - .1142\ R/L)(V/L)$ $b_4 = (.2811)\ (R/L)^{-.25} + .6450 - .1500\ R/L)(V^2/LR)$
5	$V_{y,x}$	$a_5 = a_4$ $b_5 = b_4$
6	$V_{y,rc}$	$a_6 = (1.081\ L/R + .0279 + .0685\ R/L)(V/L)$ $b_6 = (.3897\ (R/L)^{-.25} + .4567 - .0948\ R/L)(V^2/LR^2)$
7	$V_{y,rs}$	$a_7 = a_6$ $b_7 = b_6$
8	V_z	$a_8 = (2 - 2.894\ (R/L)(1 - .1383\ R/L)/(1 + 2.049\ R/L))(V/L)$ $b_8 = (2 - 3.290\ (R/L)(1 + .0270\ R/L)/(1 + 2.054\ R/L))(V^2/L)$
9	V_x	$a_9 = a_8$ $b_9 = b_8$
10	γ	$a_{10} = (.4343\ L/R + .9170 - .1532\ R/L)(V/L)$ $b_{10} = (.2579\ (R/L)^{-.25} + .6467 - .1093\ R/L)(V^2/LR)$
11	$\bar{\gamma}$	$a_{11}\ (.5342\ L/R + 1.276 - .2147\ R/L)(V/L)$ $b_{11}\ (.1167\ (R/L)^{-.25} + .7733 - .1284\ R/L)(V^2/LR)$
12	ε	$a_{12} = a_{11}$ $b_{12} = b_{11}$

* L = integral scale, R = rotor radius equation.

Discrete Time Simulation Equations

To simulate the effects of a dynamic filter, a differential equation is often simulated; this is done on a computer using a numerical approximation and involving a discrete time step. If the variables do not vary greatly over the time step chosen, the numerical approximation is considered adequate. White noise, however, contains all frequencies by definition. Therefore, no matter how small the chosen interval, the white-noise excitation will vary appreciably over the interval. This variation will destroy the accuracy of the numerical approximation.

To overcome this difficulty, we will use an analytical approach. Equation (6) can be solved analytically for piecewise continuous input and constant parameters a and b. This is done by using the classical exponential impulse response,

$$x(t+\Delta) = x(t)e^{-a\Delta} + \int_0^{\Delta} bw(t+\tau)e^{-a(\Delta-\tau)}d\tau \qquad (11)$$

where Δ is the time step. In the case when w is white noise, it is not piecewise continuous, but the integral can be interpreted as a stochastic integral (22). Applying Eq. (11) repeatedly yields the result

$$x(k+1) = \phi\ x(k) + \Gamma\ \xi(k) \qquad (12)$$

where

$$\phi = e^{-a\Delta}$$

$$\Gamma\ \xi(k) = \int_0^{\Delta} be^{-a(\Delta-\tau)}\ dw(\tau)$$

The parentheses denote evaluation at the kth time step. Because w is assumed to be Gaussian white noise, the sequence $\Gamma\xi(k)$ is found to be sequentially uncorrelated with Gaussian statistics. Thus, $\xi(k)$ can be chosen to be independent random samples from a Gaussian distribution with unit variance. The coefficient Γ is then given by

$$\Gamma = b[(1-\phi^2)\sigma^2L/(2aV^3)]^{1/2} \qquad (13)$$

where the noise power spectral density has been chosen to be σ^2L/V^3.

Computer Simulation

The discrete time model given by Eq. (12) is readily simulated on the computer. Two factors must be considered. First, because ϕ is nearly 1 for most simulation time steps, the coefficient Γ will be relatively small. Thus, as time progresses, the state variable will reflect the sum of many random increments, which, because of the law of large numbers (23), means that the state variable will be asymptotically Gaussian for a sequence $\xi(k)$ from any reasonable distribution. Thus, the $\xi(k)$ need only be roughly Gaussian for x(k) to have statistics that are much more nearly Gaussian. The second factor to consider is that many computer simulation codes allow Δ to vary from time to time. Examination of Eqs. (12) and (13) shows that ϕ and Γ must be recomputed whenever Δ is changed.

Using the discrete time model for computer simulation depends on the ability to generate sequences of independent random samples from a roughly Gaussian distribution. This roughly Gaussian distribution can be obtained by summing three random samples from a uniform distribution. Suppose ε is uniform on the interval [0,1]. Then, define

$$\xi = 2(\varepsilon_1 + \varepsilon_2 + \varepsilon_3) - 3 \qquad (14)$$

where ε_1, ε_2, and ε_3 are three independent samples from the uniform distribution. Simple results from probability theory give the mean and variance:

$$E[\varepsilon] = 2(E[\varepsilon_1] + E[\varepsilon_2] + E[\varepsilon_3]) - 3 = 0 \qquad (15)$$

$$E[\varepsilon^2] = 4(E[\varepsilon_1{}^2] + E[\varepsilon_2{}^2] + E[\varepsilon_3{}^2]) = 1 \qquad (16)$$

The independent samples from the uniform distribution can be generated on the computer using the linear congruence method. Understand that any computer procedure for generating random numbers cannot be truly random because a specific deterministic procedure is always used. Therefore, these methods are often called "pseudo-random" number generators. In particular, the linear congruence method utilizes modular arithmetic. Thus, consider

$$n(k+1) = \mathrm{Mod}[c \cdot n(k),\ m] \qquad (17)$$

where

n(k) = a sequence of integers
c = the multiplier
m = the modulus.

The function Mod(.,.) is the remainder when the first argument is divided by the second. When the sequence n(k) is examined, we find that only m different values of n are possible. Thus, the sequence will repeat at least every m times. To obtain a long period of repetition, Whitney (24) suggests that $c > \sqrt{m}$ and m must be a prime number. Uniform real numbers for the interval [0,1] are generated by the fraction

$$\varepsilon = \frac{n(k)}{m-1} \qquad (18)$$

For the particular program written here, the following values have been implemented:

$$m = 2^{31} - 1 = 2147483647$$

$$c = 46341$$

Computation is made with double-precision, floating-point arithmetic to prevent unwanted periodicities from round-off error.

The actual FORTRAN implementation of this algorithm is quite simple. Figure 2 is a flow chart that shows the calculation scheme, and Figures 3 through 6 show the FORTRAN code used to model the turbulence in the FLAP code. With this turbulence simulation scheme, the FLAP code can run a 456 revolution simulation for the Howden turbine; this can be done in 50 minutes on a Compaq 386/20 PC using a single-blade mode shape calculating loads at 10° increments. A run of 456 revolutions takes about 10 minutes of operational time for the Howden machine, so the computer simulation takes 5 times longer than the actual run time.

THE FLAP CODE

The FLAP code is a PC-based model for predicting the dynamic loads and flapping motion of an individual wind turbine blade. It accounts for the blade bending deformation about the smallest blade inertia axis. The rotor is assumed to operate at a constant speed, and the hub is allowed to move in a prescribed yawing motion. Rotors that are tilted and yawed relative to the mean wind can be analyzed. FLAP can be used to model simple teetering-rotor hubs, but not a delta-3 hinge or underslung rotors.

The model operates in the time domain, and the blade acceleration equation is integrated via a modified Euler trapezoidal predictor-corrector method. The method incorporates a set of low-order relations, is self-starting and stable, and allows frequent step-size changes. The procedure is entirely automated within the computer program. Results of the blade loads analysis are printed in tabular form and include the deflection, slope, velocity, flapwise shear and moment, edgewise shear and moment, blade tension, and blade twisting moment for any point along the blade axis.

The program, written in FORTRAN 77, is in the public domain and was developed for easy end-user modification and customization. The code contains its own documentation through the extensive use of comments within the program. Readers interested in more information concerning the FLAP code should consult (1), (2), and (25).

COMPARISON OF SIMULATIONS WITH FIELD TEST MEASUREMENTS

The FLAP code was initialized to model the Howden 330-kW horizontal-axis wind turbine located near Palm Springs, Calif., in San Gorgonio Pass. The turbine, manufactured by James Howden and Company, is a three-bladed, upwind machine with a rigid hub and wood/epoxy blades. It is rated at 330 kW in a hub-height wind speed of 32.4 mph (14.5 m/s) and was designed to operate in cut-in to cut-out wind speeds of 13.4 to 62.6 mph (6.0 to 28.0 m/s), respectively. The rotor diameter is 85.3 ft (26 m), and the rotor speed is 42 rpm. The blades are tapered and twisted, with a maximum chord of 4.8 ft (1.47 m) and a maximum twist of 16°; the blade tapered to a 2.6-ft (0.8-m) chord and 0° twist at the blade tip. The blade airfoil section is a GA(W)-1, 17% thick. The rotor axis centerline is 79.1 ft (24.1 m) above the ground, and the rotor coning angle (precone) is 0°. The tower diameter is 5.9 ft (1.8 m), and the distance from the yaw axis to the rotor plane is 11.5 ft (3.5 m).

A detailed description of the modeling inputs used for the aerodynamic and structural-dynamic parameters are given in (2). For the turbulence simulations reported here, only a single flap mode shape is used, and the natural frequency for that mode is set at 1.40 Hz (or 2P); this modeled the deterministic blade responses quite well (2). However, the gravity excitation and the wind-shear input are both set to zero to compute only the stochastic responses and the mean wind response, which is constant. The mean wind input is necessary to establish the mean angle of attack, about which turbulence causes perturbations. This approach assumes that the deterministic and stochastic response can be summed in a simple linear manner, and that there are no interaction effects. However, the validity of this assumption has never been verified.

In this paper, turbulence loads computed by FLAP are compared to measurements for three different 10-min data cases, which were taken from (26). Operating conditions for these three cases are shown in Table 2.

To compute the proper turbulence filter coefficients (using equations from Table 1) and parameters for the discrete time turbulence evolution [described in (12) and (13)], the mean wind speed V, standard deviation of wind speed σ, and integral scale L are needed. The 10-min mean is taken for V, and the standard deviation and integral scale are obtained by curve fitting (using the least-squares method) the wind-speed spectral density to the von Karman theoretical spectral density function, which is given by

$$S(\omega) = \frac{\frac{1}{\pi}\left(\frac{\sigma^2 L}{V}\right)}{\left[1 + \left(\frac{\alpha\omega L}{V}\right)^2\right]^{5/6}} \qquad (19)$$

For the curve fitting, the quantities $\frac{1}{\pi}(\sigma^2 L/V)$ and $(\alpha L/V)$ are treated as unknown parameters. Using the 10-min mean for V allowed σ and L to be computed from the curve-fit parameter values.

The hub-height wind spectrum is computed using two 5-min time-series segments and then averaging the spectral estimates. The wind time-series data were electronically filtered at 1.2 Hz to eliminate unwanted noise above the anemometer cut-off frequency. The time series were then digitized at 40 Hz for convenience and then decimated to about 6 Hz before the spectra were computed. The curve fitting is done on the average of the two 5-min spectra, but no smoothing is employed before the curve fitting.

Table 2 summarizes the standard deviation and integral scales obtained for the three data cases. Figures 7 through 9 show the computed wind spectra and the results of the curve fitting; also shown is the corresponding wind spectrum computed from the FLAP simulation for the wind as observed from the tip of the rotating blade. This comparison shows the difference between experimental and simulated results for the low-frequency region, as well as the rotational effects at 1P and 2P. The most striking feature of these curves is the large data scatter for the experimental spectral estimates. This scatter should be expected because the

Table 2. Conditions for the Three 10-Min Comparisons

Data Case	$\overline{V}$ (ft/s)	$\sigma/\overline{V}$	Mean Power (kW)	σ(ft/s)	L(ft)
12-7	34.3	0.18	169	6.2	291
3-5	31.7	0.13	119	3.6	336
17-1	55.6	0.13	298	6.6	544

$\sigma/\overline{V}$ = turbulence intensity = (standard deviation of the wind speed) ÷ (mean wind speed)

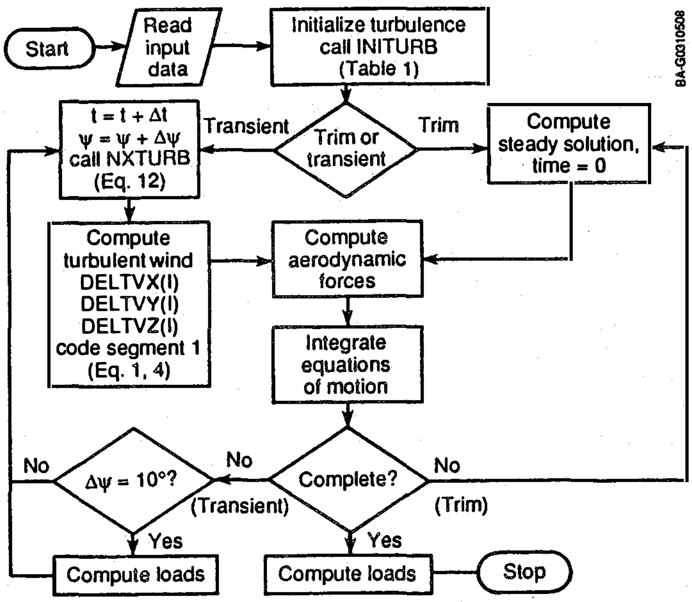

Fig. 2. Flow chart illustrating computations

```
C       ****************************************************************
C       *                                                              *
C       *   Compute the turbulent wind velocity fluctuations           *
C       *                                                              *
C       ****************************************************************



        IF(TURBON) THEN
          HRSQ = (HUBRAD+BLTIP)**2/2.
          RB= HUBRAD
          STEP = BLTIP/(NPTS-1)
          CPSI = COS(BLDANG)
          SPSI = SIN(BLDANG)
          C2PSI = COS(2.*BLDANG)
          S2PSI = SIN(2.*BLDANG)
          DO 300 I = 1,NPTS
            DELTVX(I) =TSTATE(9,1)+(TSTATE(11,1)-TSTATE(10,1))*RB*CPSI
     &                 + (TSTATE(3,1)-TSTATE(12,1))*RB*SPSI
            DELTVY(I) =TSTATE(4,1)*RB*CPSI
     &                 +TSTATE(5,1)*RB*SPSI + TSTATE(2,1)*(RB*RB-HRSQ)
     &                 +TSTATE(6,1)*RB*RB*C2PSI+TSTATE(7,1)*RB*RB*S2PSI
            DELTVZ(I) =TSTATE(8,1)+(TSTATE(3,1)+TSTATE(12,1))*RB*CPSI
     &                 + (TSTATE(11,1) + TSTATE(10,1))*RB*SPSI
            RB= RB+ STEP
  300     CONTINUE
        ENDIF


        RETURN
        END
```

Fig. 3. Code segment 1: compute turbulent wind

```
F77L - Lahey FORTRAN 77, Version 2.21   05/25/88  09:17:31
SUBROUTINE RANDOM      Compiling Options:/NA/NB/NF/H/NI/NL/NP/NR/S/NT/W/NX/NO/N7
Source file Listing
        SUBROUTINE RANDOM(DSEED,NR,R)

C       ***********************************************************
C       *  Generates nearly Gaussian random values 0.0 to 1.0.    *
C       *  The method sums three uniform random variates to       *
C       *  to obtain an approximately normal distribution.        *
C       *  DSEED = A positive integer less than DM.               *
C       *  NR    = Number of random values returned in R(NR).     *
C       *  R(NR) = The vector of NR random values.                *
C       *  DM    = 2**31-1=2147483647.DO                          *
C       *  DD    = 2**31=2147483647.DO                            *
C       *  DC    = 46341                                          *
C       ***********************************************************


        DOUBLE PRECISION DSEED
        DOUBLE PRECISION DC
        DOUBLE PRECISION DM
        DOUBLE PRECISION DD

        REAL     R(NR)
        REAL     SUM

        INTEGER  I
        INTEGER  J

        SAVE DC
        SAVE DM
        SAVE DD

        DATA DC/46341.DO/
        DATA DM/2147483647.DO/
        DATA DD/2147483648.DO/

        DO 5 I = 1,NR

          SUM = 0.0

          DO 4 J = 1,3
            DSEED = DMOD(DC*DSEED,DM)
            SUM = SUM + DSEED/DD
    4     CONTINUE

          R(I) = (SUM-1.5)*2.0

    5 CONTINUE

        RETURN
        END
```

Fig. 4. Subroutine RANDOM

```
F77L - Lahey FORTRAN 77, Version 2.21   05/25/88  09:17:31
SUBROUTINE INITRB      Compiling Options:/NA/NB/NF/H/NI/NL/NP/NR/S/NT/W/NX/NO/N7
Source file Listing
        SUBROUTINE INITRB

C       ****************************************************************
C       *  This subroutine computes the fundamental constants used     *
C       *  to simulate the turbulent velocity fluctuations.  This      *
C       *  subroutine is called from DSKREV  to compute the            *
C       *  constants.  This routine is called only once.               *
C       ****************************************************************

        REAL   ROL
        REAL   VOL
        REAL   VSQOL

        INCLUDE 'C:INCLUDE\TURBUL.INC'
        INCLUDE 'C:INCLUDE\TMODEL.INC'

        VOL = VTUR/SCALE
        VSQOL = VTUR*VOL
        ROL = DISKR/SCALE

C       Compute the A coefficients.

        TA(1) = (1.-1.713*ROL*(1.-.0790*ROL)/(1.+2.048*ROL))*VOL
        TA(2) = (1.091/ROL + .0276 + .0686*ROL)*VOL
        TA(3) = (1.654/ROL + 1.069 + 2.154 * ROL)*VOL
        TA(4) = (.3266/ROL + .5953 - .1142 * ROL)*VOL
        TA(5) = TA(4)
        TA(6) = (1.081/ROL + .0279 + .0685 * ROL)*VOL
        TA(7) = TA(6)
        T (8) = (2.-2.894*ROL *(1.-.1383*ROL)/(1.+2.049*ROL))*VOL
        TA(9) = TA(8)
        TA(10) = (.4343/ROL + .9170 - .1532 * ROL)*VOL
        TA(11) = (.5342/ROL + 1.276 - .2147 * ROL)*VOL
        TA(12) = TA(11)

C       Compute the B coeffients

        TB(1) = (SQRT(2.) - 2.713*ROL*(1.+.0159*ROL)/
     &          (1.+2.051*ROL))*VSQOL
        TB(2) = (.5508/ROL**.25 + .6473 - .1365*ROL)*VSQOL/
     &          DISKR/DISKR
        TB(3) = (.3546/ROL**.25 + .3951 + .2593*ROL)*VSQOL/DISKR
        TB(4) = (.2811/ROL**.25 + .6450 - .1500*ROL)*VSQOL/DISKR
        TB(5) = TB(4)
        TB(6) = (.3897/ROL**.25 + .4567 - .0948 * ROL)*VSQOL/
     &          DISKR/DISKR
        TB(7) = TB(6)
        TB(8) = (2.-3.290*ROL*(1.+.0270*ROL)/(1.+2.054*ROL))*VSQOL
        TB(9) = TB(8)
        TB(10) = (.2579/ROL**.25 + .6467 - .1093 * ROL)*VSQOL/DISKR
        TB(11) = (.1167/ROL**.25 + .7733 - .1284*ROL)*VSQOL/DISKR
        TB(12) = TB(11)

        RETURN
        END
```

Fig. 5. Subroutine for computing filter coefficients (VTUR = mean wind, DISKR = rotor radius, and SCALE = integral scale)

```
F77L - Lahey FORTRAN 77, Version 2.21   05/25/88  09:17:31
SUBROUTINE NXTURB      Compiling Options:/NA/NB/NF/H/NI/NL/NP/NR/S/NT/W/NX/NO/N7
Source file Listing
        SUBROUTINE NXTURB(TIMNOW)

C       ********************************************************************
C       *  This subroutine initializes the turbulence state if time is     *
C       *  zero, TIMNOW=0, or sets the constants for the turbulence state  *
C       *  if the time step, DELTAT, has been changed.  The turbulence     *
C       *  state constants are stored in the array, TSTATE(12,0:1).        *
C       ********************************************************************

        DOUBLE PRECISION DSEED

        REAL     XX

        INTEGER I

        SAVE DSEED

        INCLUDE 'C:INCLUDE\TURBUL.INC'
        INCLUDE 'C:INCLUDE\TMODEL.INC'
        INCLUDE 'C:INCLUDE\POSITN.INC'

        IF(TIMNOW.EQ.0.0.OR.DELTAT(0).NE.DELTAT(1)) THEN

          XX = SIGMA*SIGMA*SCALE/(2.*VTUR**3)

          DO 10 I = 1,12
            TPHI(I) = DEXP(-TA(I)*DELTAT(1))
            TGAM(I) = TB(I)*SQRT((1.0DO-TPHI(I)**2)*XX/TA(I))
   10     CONTINUE

        ENDIF

        IF(TIMNOW.EQ.0.0) THEN

          DSEED = SEED
          CALL RANDOM(DSEED,12,R)

          DO 25 I = 1,12
            TSTATE(I,1) = R(I)*TGAM(I)/SQRT(1.0DO-TPHI(I)**2)
   25     CONTINUE

        ELSE

          CALL RANDOM(DSEED,12,R)

          DO 35 I = 1,12
            TSTATE(I,1) = TPHI(I) * TSTATE(I,0) + TGAM(I) * R(I)
   35     CONTINUE

        ENDIF
        RETURN
        END
```

Fig. 6. Subroutine for computing turbulence state coefficients for Eqs. (1) and (4) (SIGMA = standard deviation of wind speed)

spectral estimates have been plotted unsmoothed. Usually, wind spectra are heavily smoothed by averaging several adjacent estimates or by averaging several spectral estimates from consecutive time periods. In this case, the unsmoothed spectral estimates have been used for curve fitting to obtain the best estimate for the spectrum during the 10-min time period of interest, rather than an estimate for the average atmospheric spectrum.

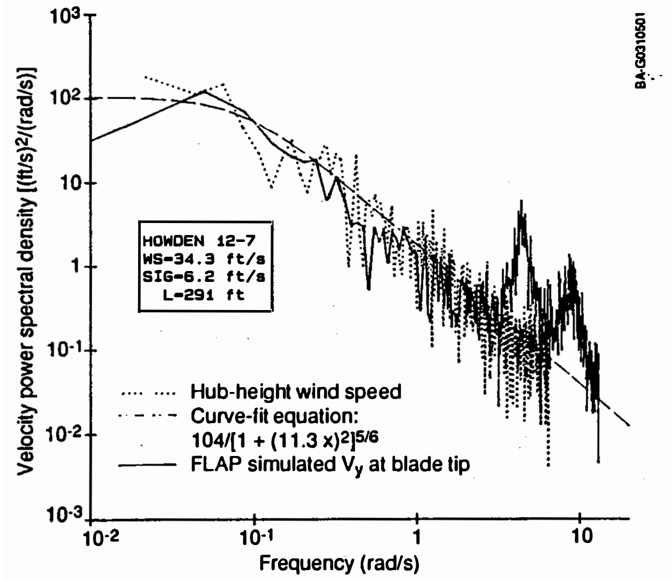

Fig. 7. Comparison of longitudinal wind spectra for case 12-7

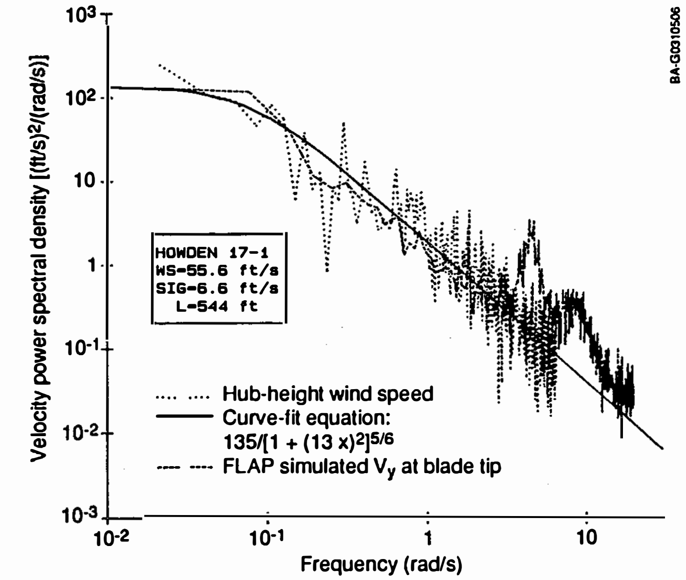

Fig. 9. Comparison of longitudinal wind spectra for case 17-1

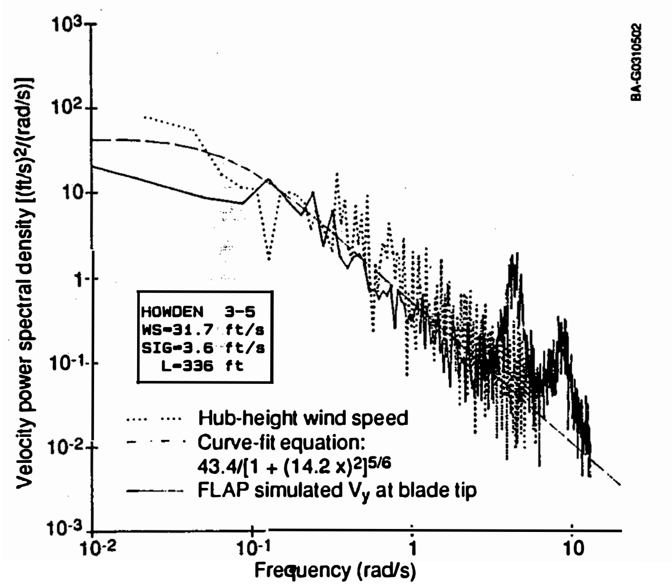

Fig. 8. Comparison of longitudinal wind spectra for case 3-5

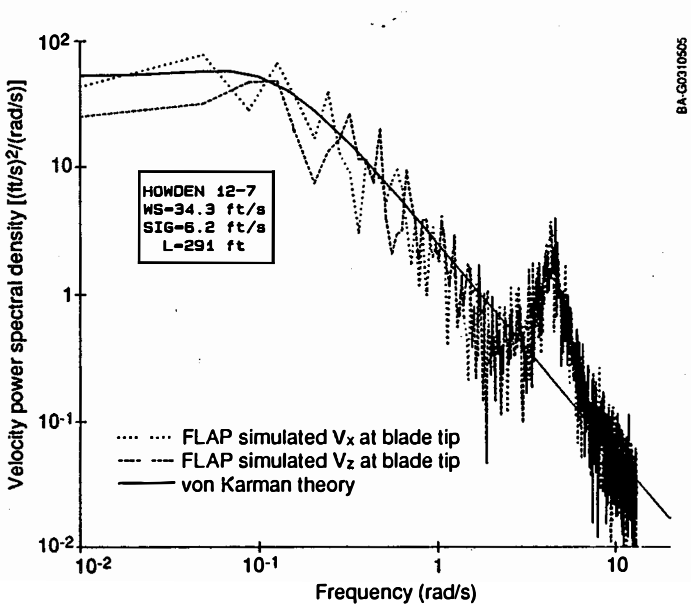

Fig. 10. FLAP simulated lateral turbulence spectra for case 12-7

The FLAP simulation results shown in Figures 7 through 9 have been smoothed by averaging three adjacent estimates; this is done primarily to reduce the data volume prior to plotting. In each of the three cases, the simulated wind spectrum agrees reasonably well with the target theoretical spectrum and the experimental data. The influence of the rotational effect is clearly seen at frequencies of 1P and 2P. The modeling neglects rotational effects at higher frequencies. Figure 10 plots the FLAP simulated lateral and vertical spectra for data case 12-7 and compares them with the theoretical von Karman spectrum that was the target.

The FLAP simulated rotor bending moments at 10% and 65% span are compared with experimental results in Figures 11 through 13. The comparison between predicted and measured results is generally quite good. The magnitudes of the major features are predicted quite well, even for the resonance at 2P. Cases 12-7 and 3-5 are for about the same wind speed; however, case 12-7 has a turbulence intensity of 18%, while case 3-5 has a turbulence intensity of about 13%. For these two cases, the pitch control system is inactive. In case 17-1, which is a high-wind-speed case, the pitch control system is active and the tips are constantly moving to control power. The FLAP code cannot model the control actions, so the agreement between predicted and measured results is not expected to be particularly good. Figure 13 shows a considerable discrepancy for the 65% span location, which is closer to the pitchable tip; however, the effect seems to average out at the 10% span. The experimental data show a response peak at about 3P that may be a tower mode excited by turbulence. The FLAP code does not model

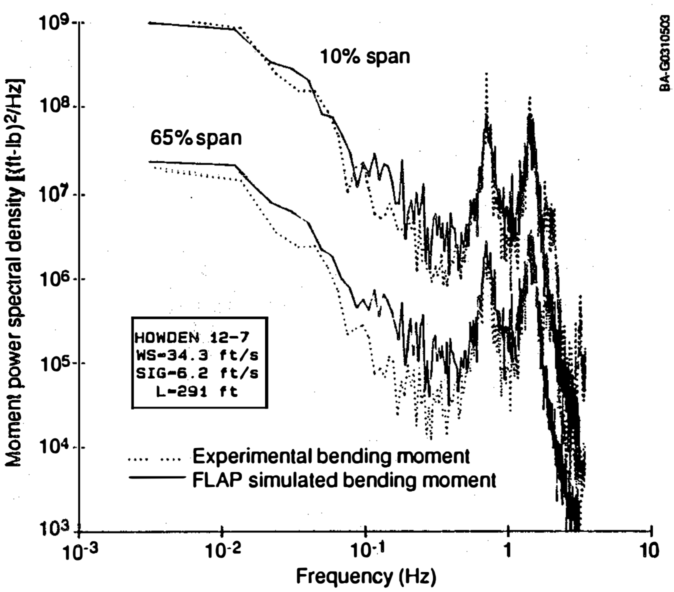

Fig. 11. FLAP simulation results for case 12-7 (for the 10% span, $\sigma_{EXP} = 1.06 \times 10^4$ ft-lb and $\sigma_{FLAP} = 1.04 \times 10^4$ ft-lb; for the 65% span, $\sigma_{EXP} = 1.72 \times 10^3$ ft-lb and $\sigma_{FLAP} = 1.85 \times 10^3$ ft-lb)

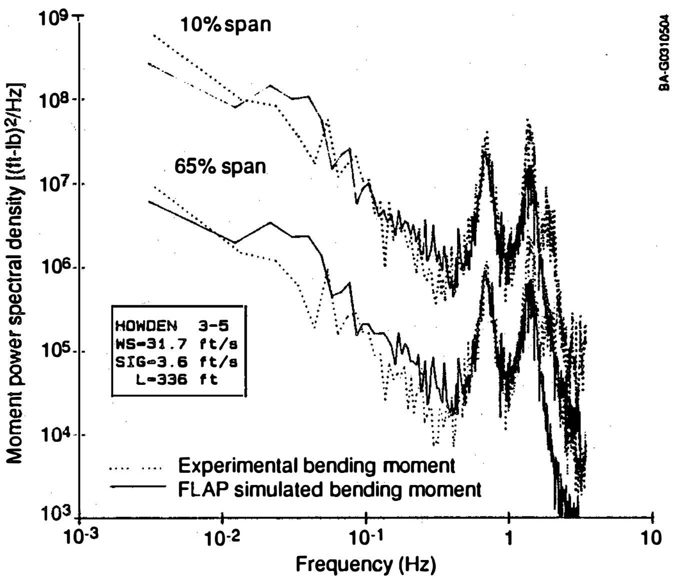

Fig. 12. FLAP simulation results for case 3-5 (for the 10% span, σ_{EXP} = 7080 ft-lb and σ_{FLAP} = 5590 ft-lb; for the 65% span, σ_{EXP} = 129 ft-lb and σ_{FLAP} = 98.9 ft-lb)

tower motions, nor does the turbulence model provide the proper input at this frequency. Therefore, this response is absent from the simulated responses. All of the structural responses have been lightly smoothed by averaging three adjacent spectral estimates before plotting.

CONCLUSIONS

The filtered-noise turbulence model has been incorporated into the FLAP code to predict turbulence-induced blade bending loads. A comparison of simulation results with experimental measurements has demonstrated that the resulting stochastic loading is predicted quite well for a rigid-hub wind turbine. The filtered-noise turbulence model as implemented in the FLAP code has proved that these simulations can be done efficiently on a personal computer. This brings the ability to estimate turbulence-induced loads within the means of all wind turbine designers.

A word of caution to potential users: The filtered-noise turbulence model as currently developed underestimates rotational wind inputs above frequencies of 2.5P. Therefore, for blades having a first flap frequency above 2.5P, or for blades with a lightly damped natural frequency above 2.5P, the resulting simulated bending moments are likely to be underpredicted. For the comparisons presented in this paper, the Howden turbine had a first flap frequency at 2P, which resulted in favorable comparisons.

The success of applying the methods described in this paper to the problem of computing a lifetime loading histogram depends on knowing the mean wind probability distribution and associated joint probabilities for both the standard deviation and the integral scale. These data are not available, even for the three major California wind sites. In addition, the spectral character of the California wind sites has not been well documented. Some feel that the spectral characteristics should resemble the text-book empirical formulas; the results of this paper don't contradict that assertion. However, the joint probabilities that define the percentage of the time that a turbine operates in high wind and high turbulence (versus high wind and low turbulence) or any other combination of conditions are still unknown.

Ultimately, the results of analyses like the one presented here must be repeated for a variety of turbulence conditions that reflect the expected lifetime environment for the turbine. The resulting loading histograms must be weighted and superposed to obtain the lifetime loading histogram from which a fatigue life estimate can be made. Although the ability to

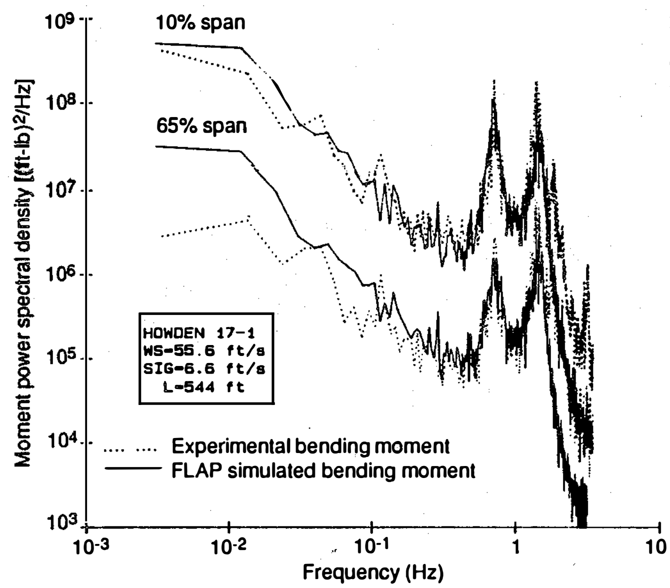

Fig. 13. FLAP simulation results for case 17-1 (for the 10% span, σ_{EXP} = 9560 ft-lb and σ_{FLAP} = 8470 ft-lb; for the 65% span, σ_{EXP} = 1870 ft-lb and σ_{FLAP} = 1740 ft-lb)

compute turbulence-induced loads is a major step forward, it is only a single step toward the final goal of a complete structural design methodology.

REFERENCES

1. Wright, A. D. and Thresher, R. W., "A Comparison of Predicted Wind Turbine Blade Loads to Test Measurements," Journal of Solar Energy Engineering, Vol. 110, No. 3, Aug. 1988, pp. 180-186.

2. Wright, A. D. and Thresher, R. W., "Accurate Rotor Loads Predictions Using the FLAP Dynamics Code," Windpower '87 Proceedings, SERI/CP-217-3315, American Wind Energy Association, Arlington, Va., 1988.

3. Holley, W. E., Thresher, R. W., and Lin, S.-R., "Atmospheric Turbulence Inputs for Horizontal Axis Wind Turbines," Proceedings of the European Wind Energy Conference, H. S. Stephens and Associates, Bedford, England, 1984.

4. Connell, J. R., "The Spectrum of Wind Speed Fluctuations Encountered by a Rotating Blade of a Wind Energy Conversion System: Observation and Theory," PNL 4083, 1981, Battelle Pacific Northwest Laboratory, Richland, Wash.

5. Kristensen, L. and Frandsen, S., "Model for Power Spectra Measured from the Moving Frame of Reference of the Blade of a Wind Turbine," Journal of Wind Engineering and Industrial Aerodynamics, Vol. 10, 1982, pp. 249-262.

6. Rosenbrock, H. H., Vibration and Stability Problems in Large Turbines Having Hinged Blades, C/T 133, 1955, ERA Technology Ltd., Surrey, England.

7. Batchelor, G. K., The Theory of Homogeneous Turbulence, Cambridge Press, Cambridge, Mass., 1953, pp. 169-187.

8. von Karman, T., "Sur la Theorie Statistique de la Turbulence," Comptes Rendus des Seanes de l'Academie de Sciences, Vol. 226, 1948, pp. 2108-2111.

9. Kolmogorov, A. N., "The Local Structure of Turbulence in Incompressible Viscous Fluid for Very Large Reynolds Numbers," Doklady ANSSSr, Vol. 30, 1941, p. 301.

10. Etkin, B., Dynamics of Atmospheric Flight, Wiley, New York, 1972, p. 539.

11. Kaimal, J. C., et al., "Spectral Characteristics of Surface Layer Turbulence," Quarerly Journal of the Royal Meteorological Society, Vol. 98, 1972, p. 565.

12. Davenport, A. G., "The Spectrum of Horizontal Gustiness Near the Ground in High Winds," Quarterly Journal of the Royal Meteorological Society, Vol. 98, 1972, p. 565.

13. Simiu, E. and Scanlan, R. H., Wind Effects on Structures, Wiley, New York, 1978, pp. 247-313.

14. Sundar, R. M. and Sullivan, J. P., "Performance of Wind Turbines in a Turbulent Atmosphere," Proceedings of the DOE/NASA Wind Turbine Dynamics Workshop, SERI/CP-635-1238, 1981, Solar Energy Research Institute, Golden, Colo.

15. Veers, P. S., "Three-Dimensional Wind Simulation," SAND-0152, March 1988, Sandia National Laboratories, Albuquerque, N. Mex.

16. Dragt, J. B., "The Spectra of Wind Speed Flutuations Met by a Rotating Blade and Resulting Load Fluctuations," Proceedings of the European Wind Energy Conference, H. S. Stephens and Associates, Bedford, England, 1984.

17. Madsen, P. M., Hock, S. M., and Hausfeld, T. E., "Turbulence Loads on the Howden 26 m Diameter Wind Turbine," Proceedings of the Seventh ASME Wind Energy Symposium, American Society of Mechanical Engineers, New York, 1988.

18. Kristensen, L. and Jensen, N. O., "Lateral Coherence in Isotropic Turbulence and in the Natural Wind," Boundary Layer Meteorology, Vol. 17, 1979, pp. 353-373.

19. Thresher, R. W., Holley, W. E., Hershberg, E. L., and Lin, S.-R., Response of the MOD-0A Wind Turbine Rotor to Turbulent Atmospheric Wind, RI/10378-82/1, 1983, Oregon State University, pp. 8-9.

20. Thresher, R. W., Holley, W. E., Smith, C. E., Jafarey, N., and Lin, S.-R., Modeling the Response of Wind Turbines to Atmospheric Turbulence, RL/2227-81/2, 1981, Oregon State University, pp. 125-131.

21. Papoulis, A., Probability, Random Variables and Stochastic Processes, McGraw-Hill, New York, 1965, pp. 515-524.

22. Ibid, pp. 323-325.

23. Ibid, pp. 263-266.

24. Whitney, C. A., "Generating and Testing Pseudorandom Numbers," Byte Magazine, October 1984, pp. 128-464.

25. Wright, A. D., Buhl, M. L., and Thresher, R. W., "FLAP Code Development and Validation," SERI/TR-217-3125, 1988, Solar Energy Research Institute, Golden, Colo.

26. Hock, S. M., Hausfeld, T. E., Hampson, G., and Thresher, R. W., "Preliminary Results from the Dynamic Response Testing of the Howden 330-kW HAWT," SERI/TP-217-3243, 1987, Solar Energy Research Institute, Golden, Colo., presented at Windpower '87, San Francisco, Calif., Oct 5-9, 1987.